24th INTERNATIONAL CONGRESS ON SOUND AND VIBRATION
23–27 July 2017, London

ICSV24
23-27JULY 2017
LONDON CALLING

THE EFFECT OF SLAT TRAILING EDGE THICKNESS ON THE NOISE FROM A 30P30N HIGHLIFT CONFIGURATION

Junhui Gao*, and Xiaodong Li
Beihang University, School of Energy & Power Engineering, Xueyuan Road 37, Beijing, China
**email: gaojhui@buaa.edu.cn*

Dakai Lin
Beijing Aeronautical Science & Technology Research Institute of COMAC, Beijing 102211, China

In this study the noise generated by the 30P30N highlift airfoil is simulated with a high order computational aeroacoustics code using Detached Eddy Simulation method. To handle the complex geometry of the airfoil, the high order spectral difference method based on unstructured mesh is used for spatial discretization. The multi-time-step method based on Adam-Bashforth scheme is utilized for time marching. In this simulation, the inflow Mach number is 0.17, and the Reynolds number based on the inflow velocity and the chord length of the airfoil is 1.7×10^6. An attack angel with 5.5 degree is considered. Three cases for the slat with different trailing edge thicknesses are computed. The dynamic pressure on the surface of the slat is sampled and compared with the experimental data by other researchers, and a good agreement is obtained. The far field noise, computed with the permeable Ffowcs Williams-Hawkings (FW-H) integration method, is analyzed and compared with the experimental data.

Keywords: High-lift configuration, slat trailing edge thickness, spectral difference method, noise

1. Introduction

The increasingly use of high bypass turbo-fan aero-engines makes the jet noise reduced greatly. Therefore the airframe noise is more important, especially during their approach for landing. Actually the level of airframe noise is comparative with the jet noise in landing. The noise generated by the high-lift configuration device is one of the dominant components of the airframe noise. There are three noise sources for the high-lift device: the slat noise, the trailing edge noise and the flap side edge noise. The mechanism of the noise from the high-lift configuration is very complicated because of the complex flow. Many researchers [14, 15, 17, 18, 19] studied the noise of the high-lift configuration experimentally, and provided useful aerodynamic and aeroacoustic data. These works helped us to understand the mechanism of high-lift noise, especially the slat noise. With the fast development of the computers and the computational aeroacoustics, numerical simulation is becoming a valuable tool in slat noise investigation. More and more researcher [10, 11] studied the slat noise numerically with various numerical methods, for example, unsteady RANS [10], Large-Eddy simulation, Detached-Eddy simulation [16] or Zonal LES/RANS methods [11]. To validate the numerical methods for airframe noise prediction, the workshop for airframe noise computations (BANC) has been conducted 4 times from 2010 to 2016. The slat noise from a 30P30N high-lift device is a benchmark problem for all BANC-I to IV. The objective of the present study is aimed at predicting accurately the noise from a 30P30N high-lift configuration with a high-order spectral difference solver, and studying the effects of the slat trailing edge thickness on the far field noise.

In the next section, the numerical method is introduced briefly. The numerical results are presented in section 3. Section 4 gives the conclusion of this work.

2. Numerical methods

In this study, the 3D unsteady Reynolds-Averaged Navier-Stokes equations in conservative form are solved with the spectral difference method [1] on hexahedral element. The details of the governing equations and SD method are not presented here for brevity. The Delayed DES method [2] based on a modified SA model [3] is implemented to the current SD solver, and validated with a series of benchmark problems [4]. The multi-time step method [6] based on the optimized Adams-Bashforth scheme [7] is implemented in the SD solver for time integration to speed up the simulation. The spectral difference solver with multi-time-step method was validated by the present authors and applied to simulate aeroacoustics problems with multiple flow scales [8, 5]. The results demonstrated that the multi-time-step method is accurate and efficient for unsteady flow simulation with multiple scales.

Boundary condition is an key element of CAA. In this study, the radiation boundary condition by Tam & Dong [9] is used in the upstream and far field region. At the downstream boundary region, the outflow boundary condition proposed by Tam & Dong [9] is applied. The no-slip boundary condition is applied on the airfoil surfaces. For the SA turbulence model, the eddy viscosity ($\tilde{\nu}$) is set to be zero on the wall. Periodic boundary condition is used in the span-wise direction.

3. Results

In this study, the 30P30N high-lift configuration is used for simulation. The geometry of the device is plotted in Fig. 1. Three slats with different trailing edge thicknesses are considered in this study, as shown in zoom view of the slat trailing edge in Fig. 1, which are $0, \Delta/2$ and Δ respectively, where $\Delta = 5.6mm$. In the simulation, the inflow Mach number is 0.17, and the Reynolds number based on the inflow velocity and the chord length (C) of the airfoil is 1.7×10^6. The attack angle equal to 5.5 degree is considered in this study.

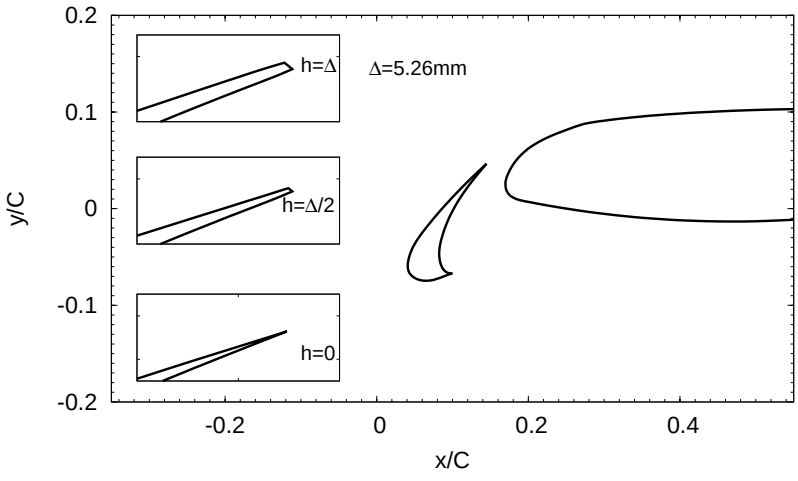

Figure 1: The geometry of the 30P30N high-lift configuration

The computational domain is extended to about $6C$ in the upstream and radial directions, and $11C$ in the downstream direction. To reduce the computation resource, the span-wise length of the airfoil is $L_z = 0.2C$. According to Lockard & Choudhari [10], Deck & Laraufie [11], a spanwise extent of $0.8c_s$ is necessary to get a proper span-wise de-correlation of the slat cove flow, where c_s is the length of slat and equal to $0.15C$. The mesh used in the simulation is shown in Fig. 2. Totally there are about 340,000 hexahedral elements, and 10 elements are distributed uniformly in the span-wise

direction. To utilize the multi-time-step method, the mesh is parted into 6 sub-domains according to the cell sizes. The speed-up ratio is about 10 for a parallel computation with 224 cores.

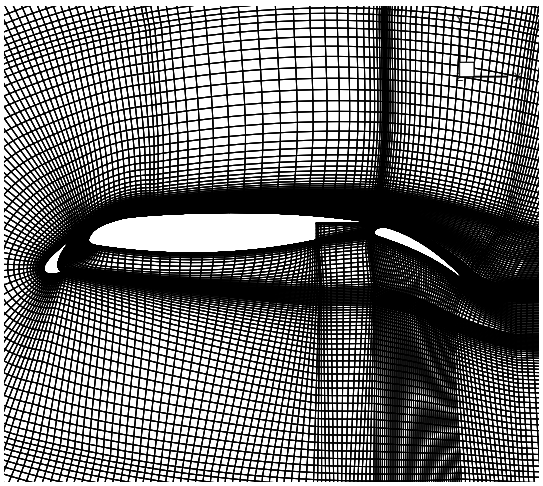

Figure 2: Part of mesh used in the simulation.

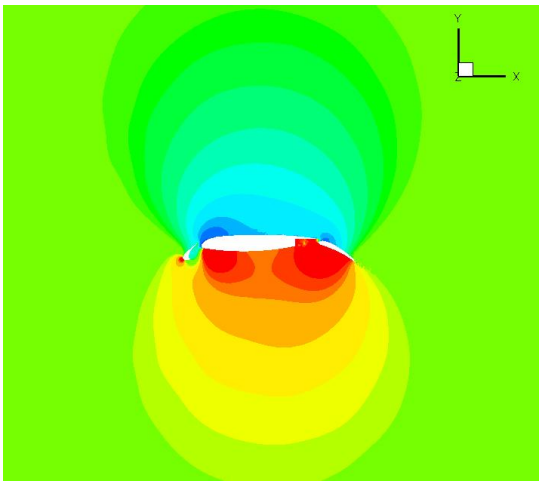

Figure 3: Instantaneous pressure field of high-lift configuration in $x-y$ plane.

3.1 Flow field

The instantaneous pressure field in $x-y$ plane of airfoil at 5.5^o angle of attack is plotted in Fig. 3. It is clear that a pressure pattern of dipole source can be observed. The vortical structures of the high-lift configuration at 5.5^o angle of attack is shown in Fig. 4. The vorticities are identified with the Q vortex criteria. A large recirculation bubble bounded by a shear layer emanating from the slat cusp and re-attaching near the slat trailing edge is clearly observed in the cove of the slat, which is shown in Fig. 4(b). Also many small scale structures is full of the cove of the slat. The flow passing the slat gap is accelerated highly, and the vorticities close to the slat trailing edge are distorted greatly to be long tubes. The mean flow field is obtained with a long time average. The contours of the mean

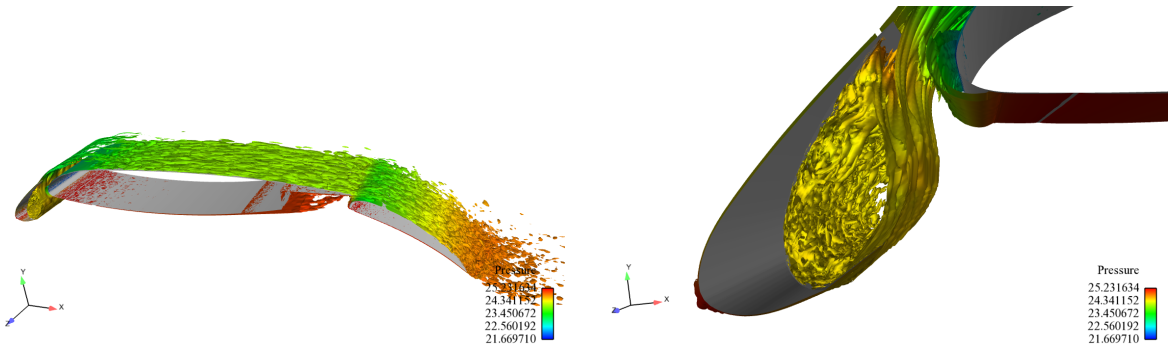

(a) (b)

Figure 4: Iso-surface of $Q = -1000$ colored by the velocity((a) whole, (b) slat).

velocities in the cove of the slat for the airfoil at $AoA = 5.5^o$ are plotted in Fig. 5. The experimental results by Jenkins et al. [13] are also presented for comparison. It is found that the numerical results are very close to the experimental data both for the streamwise and vertical velocities. The mean velocity magnitude profiles in the shear layer of the slat cove are plotted in Fig. 6 for the airfoil at 5.5^o angle of attack. The locations of the data sampling are shown in Fig. 6(a). The computed velocity magnitude profiles are compared with the PIV data by pascioni et al. [18]. The numerical results agree relatively well with the experimental data. This indicates that the numerical simulation

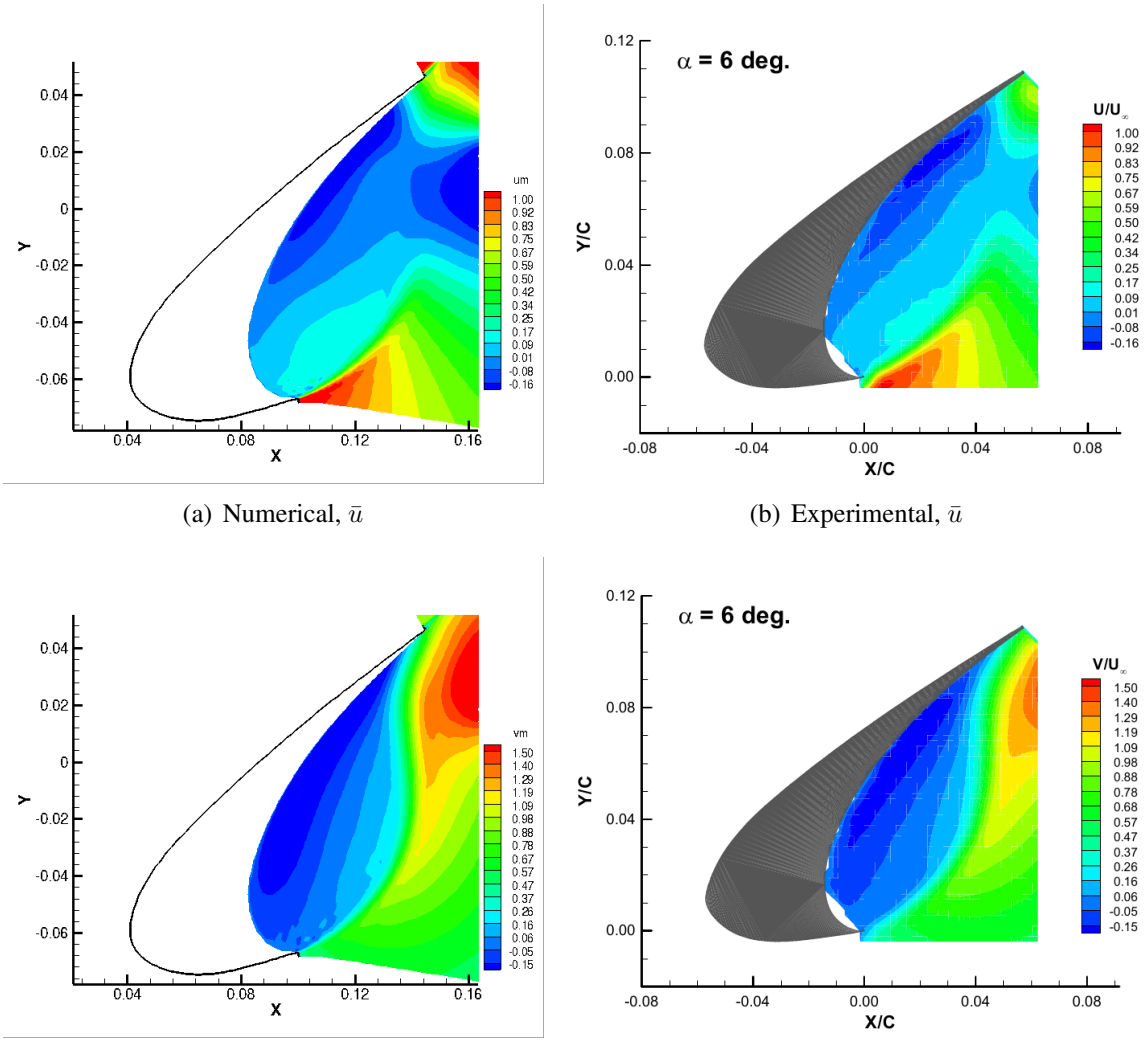

(a) Numerical, $\bar{u}$

(b) Experimental, $\bar{u}$

(c) Numerical, $\bar{v}$

(d) Experimental, $\bar{v}$

Figure 5: Comparison of the mean flow velocity in the cove of the slat.

computed the flow field correctly. The pressure coefficients on the surface of the three-element airfoil

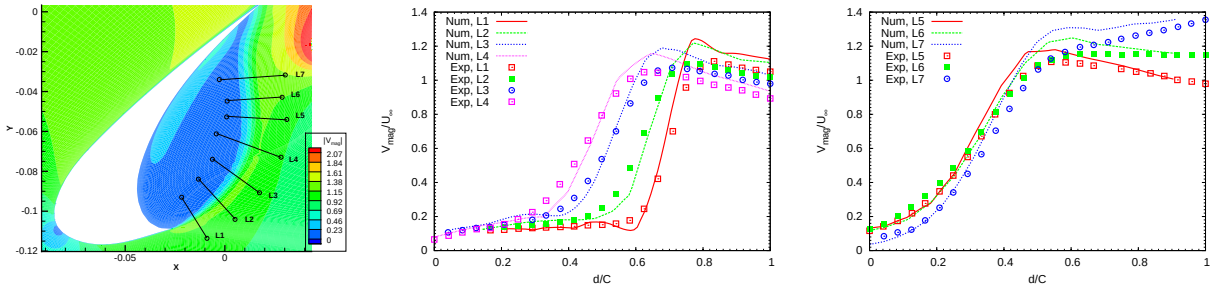

(a) Locations (b) Velocity profiles at L1 to L4 (c) Velocity profiles at L5 to L7

Figure 6: Mean velocity magnitude profiles in the shear layer of the slat cove.

at 5.5^o angle of attack are plotted in Fig. 7. The results with different slat trailing edge thicknesses are presented and compared with each other. The numerical results are compared with the experimental data of FSU [18] and JAXA [19]. The difference is clear for results on the slat surface. The results of the case with thickness $h = 0$ deviate from the experimental data more than the other two cases. The difference is small for the results on the main and flap surfaces for the three cases because the unchanged geometry. The results of the case with thickness $h = \Delta/2$ agree much better with the experimental data of JAXA than others, especially for the results on the suction side of the slat cove. Generally speaking, the computed pressure coefficients on the surfaces of the three elements agree well with the experimental data of JAXA [19] than FSU [18]. The computed lift and drag coefficients

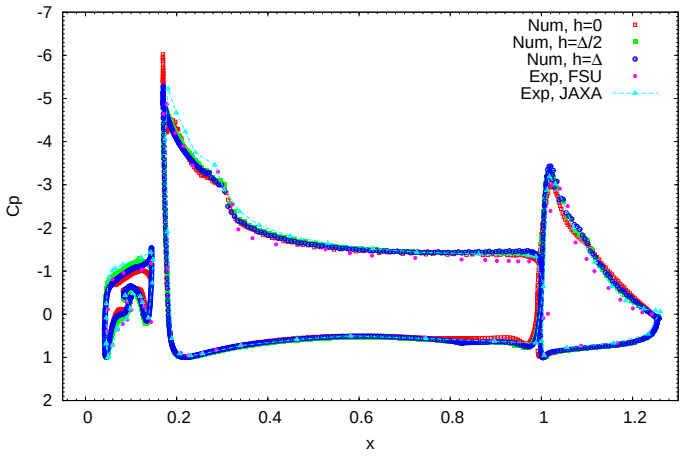

Figure 7: The pressure coefficients on the airfoil surface, compared with the experimental data of FSU [18] and JAXA [19].

are presented in Tab. 1 for the three cases. The forces of each element are given separately to show the effect of the slat trailing edge thickness on the forces. It is found that the case with $h = \Delta/2$ has largest forces, both for the slat and the whole high-lift configuration.

3.2 Dynamic pressure and far-field noise

The dynamic pressure on the surface of the slat cove is sampled nearby the re-attachment point for analysis. The position for data sampling is shown in Fig. 8. The power spectral density (PSD) of the dynamic pressure is computed and plotted in Fig. 9. The numerical results are compared with the experimental data by Pascioni et al. in FSU [18]. It is clear that the numerical simulation captured both the broadband and tonal components. The numerical results agree well with the experimental

Table 1: Lift and drag coefficients.

case		slat	main	flap	total
$h = 0$	lift	0.07344	2.02851	0.53608	2.63803
	drag	-0.00375	-0.33202	0.21487	-0.120897
$h = \Delta/2$	lift	0.104227	2.04474	0.50614	2.65511
	drag	-0.040796	-0.32539	0.22323	-0.14296
$h = \Delta$	lift	0.08681	2.00856	0.50478	2.60015
	drag	-0.02020	-0.31790	0.22573	-0.11237

data in the mid frequency range because of the grid resolution limit. A better agreement in the high frequency range requires much more grid points or higher order SD scheme. Comparing the results with different slat trailing edge thicknesses, it is found that a peak with central frequency close to 20 is appeared in the spectra for the case with $h = \Delta$. A much smaller peak with higher frequency can also be observed in the spectra for the case with $h = \Delta/2$. This is possibly related to the vortex shedding in the wake of slat. The remaining spectral features remain unchanged for the three cases.

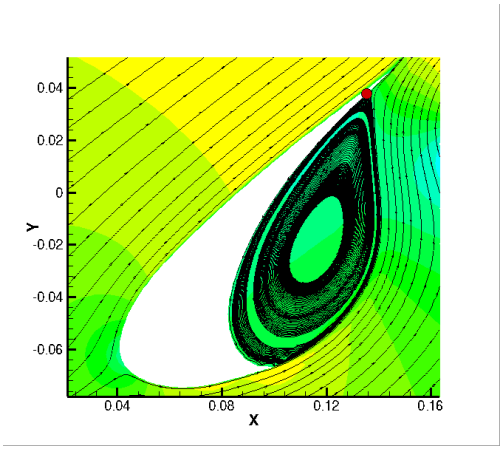

Figure 8: Position of dynamic pressure sampling in the cove of the slat.

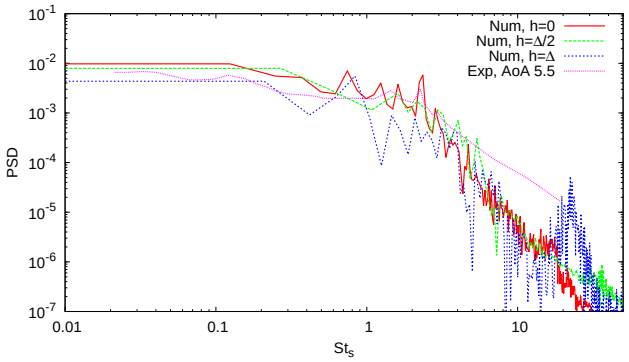

Figure 9: PSD of the dynamic pressure on the surface of the slat cove.

A surface enclosing the airfoil in the near field is used to sample the data. The data are saved in a long enough time for calculating the far field noise with FW-H integration. The noise spectra in the direction of 290^o at $10C$ away are plotted in Fig. 10. The reference results calculated with Guo's model [20] are also presented for comparison. It is found that the numerical results agree well with Guo's model. It also can be found that the high-frequency roll-off in far-field acoustic spectra appears similar to the $f^{-2.8}$ decay according to the empirical model of Pott-Pollenske et al.[14]. At low frequency range from 0.2 to 1, the power spectral density in Fig. 10 decreases with the Strouhal number, which is very close to weak decay $f^{-0.7}$ predicted by the empirical model [14]. A component with frequency close to 20 appears in the spectra for the slat with trailing edge thickness equal to Δ. A component with higher frequency can also be found in the spectra of the slat with trailing edge thickness decreased half. The frequency of the peak increases with the decreases of the thickness of the slat trailing edge. The remaining spectral features remain unchanged for the three airfoils. Mendoza & Brooks [17] investigated the effects of slat trailing edge thickness on the slat noise experimentally, and similar results were obtained in their study. This implies that the high frequency component is related to the trailing edge thickness, and is possibly generated by the vortex shedding of the trailing edge.

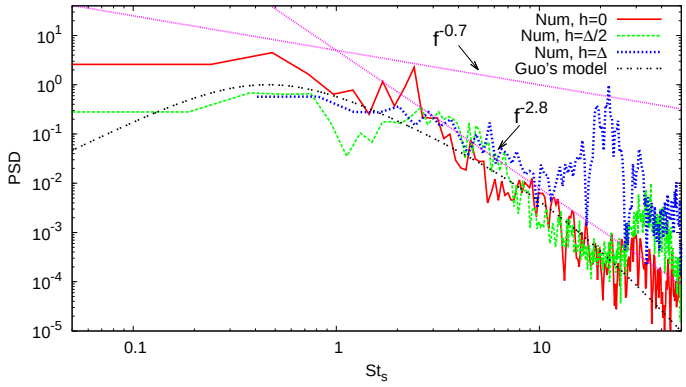

Figure 10: Far field noise PSD of high-lift configuration at $AoA = 5.5^o$

4. Conclusions

In this study the noise generated by a 30P30N highlift airfoil with 5.5 degree angle of attack is simulated with a high order spectral difference solver coupling detached eddy simulation method based on SA model. Three cases with different slat trailing edge thickness are considered in this study. The time averaged mean flow fields, including the velocity profiles in the shear layer of the slat cove, the pressure coefficient on the surface of the airfoil, are compared with the experimental data. The good agreement implies that the numerical simulation is accurate. The dynamic pressure on the surface of the slat cove, which is close to the re-attachment point, is sampled and analyzed. The computed PSD agrees well with the experimental data of Jenkins et al. in a relative large frequency range. The far field noise, computed with the permeable Ffowcs Williams-Hawkings integration method, is analyzed and compared with the experimental data and the prediction result with Guo's model, and a good agreement is obtained. A high frequency component related with the vortex shedding of the slat trailing edge appears in the spectra for the cases with non-zero thickness of the slat trailing edge, and the remaining spectral features remain unchanged. The frequency of the peak increases with the decreases of the slat trailing edge thickness.

Acknowledgments

This work is supported by grants from NSFC-51376015, NSFC-51411130130, and the Aeronautical Science Foundation of China (2014ZB51023).

REFERENCES

1. Sun, Y., Wang, Z. J., and Liu, Y., High-order Multidomain Spectral Difference Method for the Navier-Stokes Equations on Unstructured Hexahedral Grids, *Communications in Computational Physics*, **5**, 760–778 (2009).

2. Spalart, P. R., Deck, S., Shur, M. L., Squires, K. D., Strelets, M. K., and Travin, A., A New Version of Detached-eddy Simulation, Resistant to Ambiguous Grid Densities, *Theoretical and Computational Fluid Dynamics*, **20**, 181–195 (2006).

3. Crivellini, A., D'Alessandro, V., and Bassi, F., A Spalart-Allmaras Turbulence Model Implementation in a Discontinuous Galerkin Solver for Incompressible Flows, *Journal of Computational Physics*, **241**, 388–415 (2013).

4. Gao, J. H. and Li, X. D., Detached Eddy Simulation of Flow over NACA0012 Airfoil at High Angle of Attack with Spectral Difference Method, *52nd AIAA Aerospace Sciences Meeting*, AIAA Paper 2014–0425 (2014).

5. Gao, J. H. and Li, X. D., Numerical Simulation of the Noise from Tandem Cylinder Flow with Spectral Difference Method, *54th AIAA Aerospace Sciences Meeting*, AIAA Paper 2016–0265 (2016).

6. Lin, D., Jiang, M., and Li, X., A Multi-Time-Step Strategy based on an Optimized Time Interpolation Scheme for Overset Grids, *Journal of Computational Acoustics*, **18**, 131–148 (2010).

7. Tam, C. K. W. and Webb, J. C., Dispersion-Relation-Preserving Finite Difference Schemes for Computational Acoustics, *Journal of Computational Physics*, **107**, 262–281 (1993).

8. Gao, J. H. and Li, X. D., A Multi-Time-Step Spectral Difference Solver for Multiple-Scales Aeroacoustics Problems, *the 21^{s}t International Congress on Sound and Vibration*, July 13-17, 2014, Beijing, China (2014).

9. Tam, C. K. W. and Dong, Z., Radiation and Outflow Boundary Conditions for Direct Computation of Acoustic and Flow Disturbances in a Nonuniform Mean Flow, *Journal of Computational Acoustics*, **4**, 175–201 (1996).

10. Lockard, D.P., and Choudhari, M., Noise Radiation from a Leading-Edge Slat, 2009, AIAA Paper 2009-3101.

11. Deck, S., and Laraufie, R., Numerical Investigation of the Flow Dynamics past a Three-Element Aerofoil, *Journal of Fluid Mechanics*, **732**, 401–444, (2013).

12. Terracol, M., manoha, E., and Lemoine, B., Investigation of the Unsteady Flow and Noise Generation in a Slat Cove, *AIAA Journal*, **54**, 469–488 (2016).

13. Jenkins, L.N., Khorrami, M.R., Choudhari, M., Characterization of unsteady flow structures near leading-edge slat: Part I. PIV Measurements, *Proceedings of the 10th AIAA/CEAS Aeroacoustics Conference*, AIAA Paper 2004–2802, (2004).

14. Pott-Pollenske, M., Dobrzynski, W., Buchholz, H., Gehlhar, B., and Walle,F., Validation of Semi-empirical Airframe Noise Prediction Method through Dedicated A319 Flyover Noise Measurements, AIAA Paper 2000–2470 (2000).

15. Dobrzynski, W., and Pott-Pollenske, M., Slat Noise source Studies for Farfield Noise Prediction, *Proceedings of the 7th AIAA/CEAS Aeroacoustics Conference*, AIAA Paper 2001-2158 (2001).

16. Knacke, T., and Thiele, F., Numerical Analysis of Slat Noise Generation, *Proceedings of the 19th AIAA/CEAS Aeroacoustics Conference*, AIAA Paper 2013–2162 (2013)

17. Mendoza, J. M., and Brooks, T. F., Aeroacoustic Measurements of A Wing/Slat Model, *Proceedings of the 8th AIAA/CEAS Aeroacoustics Conference*, AIAA Paper 2002–2604 (2002).

18. Pascioni, K.A., Cattafesta, L.N., Choudhari, M.M, An Experimental Investigation of the 30P30N Multi-Element High-Lift Airfoil, *Proceedings of the 20th AIAA/CEAS Aeroacoustics Conference*, AIAA Paper 2014–3062, (2014).

19. Murayama, M., Nakakita, K., Yamamoto, K., Ura, H., adn Ito, Y., Experimental Study of Slat Noise from 30P30N Three-Element High-Lift Airfoil in JAXA Hard-Wall Low-Speed Wind Tunnel, *Proceedings of the 20th AIAA/CEAS Aeroacoustics Conference*, AIAA Paper 2014–2080 (2014).

20. Guo, Y.P., Slat Noise Modeling and Prediction, *Journal of Sound and Vibration*, **331**, 3567–3586 (2012).